Influence of ^{73}Rb on the ashes of accreting neutron stars

D. E. M. Hoff,[1,*] A. M. Rogers,[1,†] Z. Meisel,[2] P. C. Bender,[1] K. Brandenburg,[2] K. Childers,[3,4] J. A. Clark,[5] A. C. Dombos,[3,6,7] E. R. Doucet,[1] S. Jin,[3,6,7] R. Lewis,[3,4] S. N. Liddick,[3,4] C. J. Lister,[1] C. Morse,[1,‡] H. Schatz,[3,6,7] K. Schmidt,[3,7,§] D. Soltesz,[2] S. K. Subedi,[2] S. M. Wang (王思敏),[3] and S. Waniganeththi[1]

[1]*Department of Physics and Applied Physics, University of Massachusetts Lowell, Lowell, Massachusetts 01854, USA*
[2]*Institute of Nuclear and Particle Physics, Department of Physics and Astronomy, Ohio University, Athens, Ohio 45701, USA*
[3]*National Superconducting Cyclotron Laboratory, Michigan State University, East Lansing, Michigan 48824, USA*
[4]*Department of Chemistry, Michigan State University, East Lansing, Michigan 48824, USA*
[5]*Physics Division, Argonne National Laboratory, Argonne, Illinois 60439, USA*
[6]*Department of Physics and Astronomy, Michigan State University, East Lansing, Michigan 48824, USA*
[7]*JINA-CEE, Michigan State University, East Lansing, Michigan 48824, USA*

(Received 1 July 2020; accepted 28 September 2020; published 20 October 2020)

We find that the proton separation energy, $S(p)$, of ^{73}Rb is $-640(40)$ keV, deduced from the observation of β-delayed ground-state protons following the decay of ^{73}Sr. This lower-limit determination of the proton separation energy of ^{73}Rb coupled with previous upper limits from nonobservation, provides a full constraint on the mass excess with $\Delta M(^{73}\mathrm{Rb}) = -46.01 \pm 0.04$ MeV. With this new mass excess and the excitation energy of the $J^\pi = 5/2^-$ isobaric-analog state ($T = 3/2$) in ^{73}Rb, an improved constraint can be put on the mass excess of ^{73}Sr using the isobaric-multiplet mass equation (IMME), and we find $\Delta M(^{73}\mathrm{Sr}) = -31.98 \pm 0.37$ MeV. These new data were then used to study the composition of ashes on accreting neutron stars following Type I x-ray bursts. Counterintuitively, we find that there should be an enhanced fraction of $A > 102$ nuclei with more negative proton separation energies at the ^{72}Kr *rp*-process waiting point. Larger impurities of heavier nuclei in the ashes of accreting neutron stars will impact the cooling models for such astrophysical scenarios.

DOI: 10.1103/PhysRevC.102.045810

I. INTRODUCTION

Nuclear structure along the proton dripline has a large impact on the astrophysical rapid-proton capture (rp) process, which is thought to drive thermonuclear explosions on the surface of accreting neutron stars producing x-ray bursts [1–6]. The rp process involves thousands of reactions on hundreds of nuclides, but only the properties of a subset of nuclides have consequential impacts on the x-ray burst properties, including the light curve and the composition of synthesized nuclides otherwise known as the ashes. Some of the most consequential nuclides are the so-called waiting points, which each form a bottleneck in the rp process [2,3,7]. Waiting points occur when the rp process converges on a nucleus that does not have a rapid mechanism for destruction, which typically implies a small or negative proton-capture Q value and a β-decay half-life of several seconds. The proton-capture Q value for the waiting point, or rather the proton separation energy $S(p)$ of the proton-capture product, plays a particularly strong role in determining the strength of the waiting point. As such, a number of studies in recent years have focused on constraining $S(p)$ related to known or suspected rp-process waiting points [8–14].

While the x-ray burst light curve has been the prime motivation for rp-process studies for the last three decades, recently the x-ray burst ashes have become of renewed interest (e.g., Refs. [15–17]). Because the nuclides synthesized in the burst for the most part lack the energy to escape the gravitational pull of the underlying neutron star, although in certain scenarios some of the ashes may be carried away by a radiation-driven wind [18], the burst ashes significantly shape the structure of the neutron star crust, influencing the associated observables [6]. As with the x-ray burst light curve, the properties of waiting-point nuclides are known to have an outsize effect on the overall ash composition [3,19].

The particle-unbound nature of ^{73}Rb has been established by several previous experiments [20–22], and thus ^{72}Kr was identified as a potential waiting point in the rp process. However, this unbound nature has prevented a direct determination of its ground state energy, and thus the extent to which ^{72}Kr is a waiting point. Here we access states in ^{73}Rb and measure the proton separation energy using the energy of protons emitted from the ground state via the β-delayed proton decay of ^{73}Sr. The β-delayed proton emission spectrum of ^{73}Sr from this experiment was recently presented in a previous article [23], however the focus was on the nuclear structure of ^{73}Rb

*daniel_hoff@uml.edu
†andrew_rogers@uml.edu
‡Present address: Nuclear Science Division, Lawrence Berkeley National Laboratory, Berkeley, CA 94720.
§Present address: Institute of Radiation Physics, Helmholtz-Zentrum Dresden-Rossendorf, 01328 Dresden, Germany.

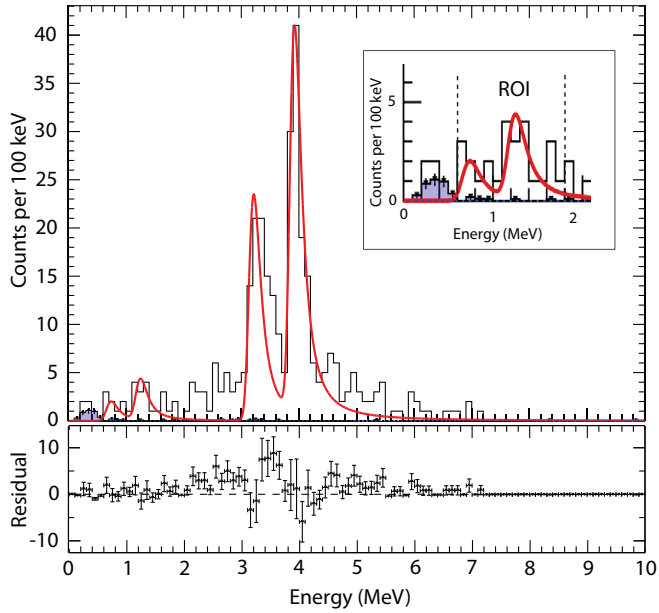

FIG. 1. The solid black histogram shows the β-delayed proton spectrum of ^{73}Sr. The fits to the proton decay of ^{73}Rb*(IAS) measured previously, as well as the peaks from the Bayesian analysis performed on the unbinned data are shown as a solid red line. The residuals taken from subtracting the measured background (indicated by the blue shaded region) and fits are also shown. The inset shows the particular region of interest (ROI) for this study.

and ^{73}Sr highlighting isobaric-spin symmetry breaking in the $T = 3/2$ quartet along the $A = 73$ isobar chain. In this article we present a study on the proton separation energy of ^{73}Rb as well as the resulting effects on the predicted composition for neutron-star crusts of accreting neutron stars in x-ray burst scenarios.

II. EXPERIMENT

The experiment was performed at the National Superconducting Cyclotron Laboratory, using a primary 140-MeV/nucleon ^{92}Mo beam fragmented on a 152.2-mg/cm^2 Be target and passed through the A1900 fragment separator selecting for ^{73}Sr [24]. The secondary ^{73}Sr beam was further purified by a factor of 4500 after passing through the radiofrequency fragment separator [25], and the remaining ions were sent through a telescope stack and implanted into a double-sided silicon strip detector (DSSSD) as detailed in Ref. [23].

For the mass of ^{73}Rb, the key part of the β-delayed proton spectrum is at low energy, below 1.5 MeV. In order to produce the cleanest spectrum in this energy domain a stringent selection with event-by-event pulse shape selection was used (see Supplemental Material, Ref. [26]) which was not included in our previous analysis [23]. By removing noisy malformed pulses the low energy background was reduced and the resulting β-delayed proton spectrum generated is shown in Fig. 1. The spectrum is subtly different from our previous article [23], however it does not shift the higher energy peaks associated with the decay of the isobaric-analog state (IAS), nor is there any statistically significant difference in the reported branching ratios even though several more decay events of ^{73}Sr were found.

The two largest peaks in Fig. 1 are attributed to proton decays from the resulting IAS in ^{73}Rb populated in the β decay of ^{73}Sr, as discussed in detail in Ref. [23]. The background in the low-energy region, however, prevented identification of weakly fed states with low-energy proton decay events. With the reduced background, there is a statistically significant signal just above 600 keV in Fig. 1. In the region of interest from 0.6–1.8 MeV (labeled ROI and highlighted by the inset of Fig. 1), this lowest-energy peak is attributed to direct decays from the ground state of ^{73}Rb to the ground state of ^{72}Kr, providing a measure of the proton separation energy.

The counts below 600 keV are well explained by the measured β background originating predominately from the $\beta + \gamma$ decay channel of implanted ^{71}Kr, the largest beam contaminant implanted into the silicon detector. The placement of the lowest-energy peak was determined through a Bayesian analysis detailed below, and the residual was generated by subtracting the measured background as well as the model peaks.

III. BAYESIAN ANALYSIS

Due to the low number of counts within the ROI of Fig. 1, a Bayesian analysis was carried out to determine the uncertainty of the ground-state peak energy, as well as assess the possible contribution of a second transition in the ground-state peak. The Bayesian analysis was performed using the Markov chain Monte Carlo method (MCMC), with the EMCEE PYTHON package (v3.0.2) [27]. Instead of the typical χ^2 analysis on binned data, where the likelihood is modeled by $e^{-\chi^2/2}$, a direct likelihood function was generated for the unbinned data points that does not incorporate a background model, requiring a low-background spectrum in the ROI, using the probability density function of the expected detector response. The functional form of the detector response was taken from the Landau distribution, convoluted with a Gaussian distribution of the measured silicon detector resolution, fit to the largest peak in the spectrum (the IAS$\rightarrow$ ^{72}Kr g.s. transition) as outlined in Ref. [23]. Only the peak positions and relative intensities were considered in the analysis. A uniform prior was assumed within the ROI. Figure 2(a) shows the result of the Bayesian analysis when considering two peaks within the ROI. Our data support a peak at $E = 1250$ keV, and a peak at $E = 740$ keV. For presentation in Fig. 1, the absolute intensity was found from the number of counts in the region of interest. To investigate if there was any evidence for an additional peak, another peak was added to the model. The intensity parameter for the additional peak was introduced in such a way that the original parameters could be directly compared, i.e. the original model is nested in the newer model. As can be seen from Fig. 2(b), the third peak is poorly constrained, and this is confirmed by comparing the Bayesian evidence between the models.

To compare the two models, one with two peaks (doublet) and with three peaks (triplet), the Bayes factor for each model was calculated via thermodynamic annealing (or integration)

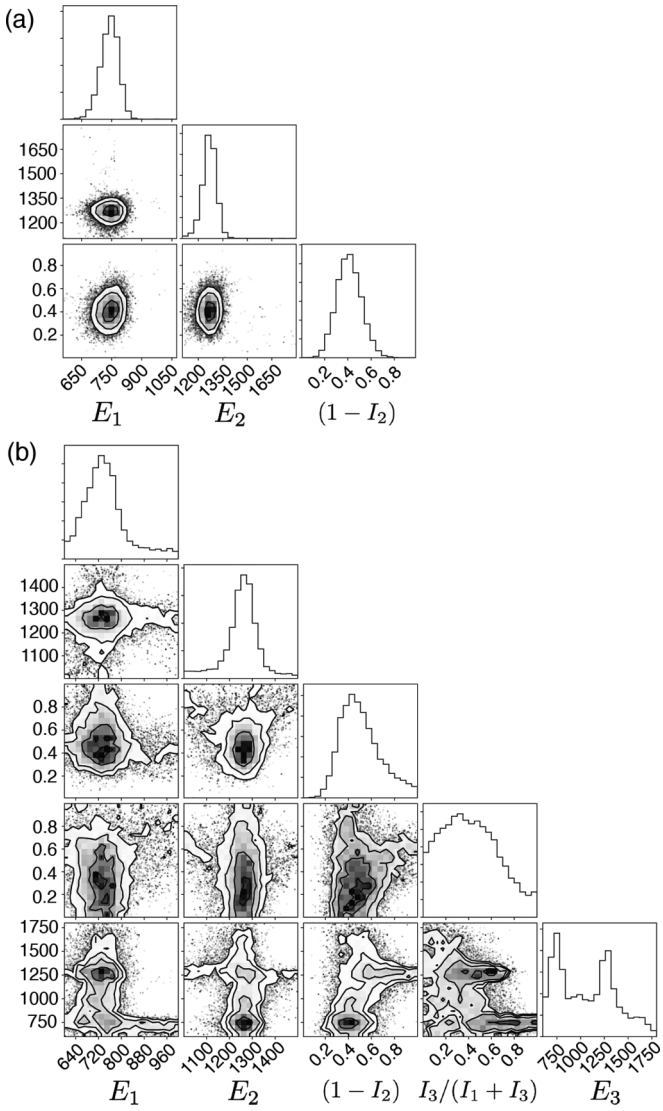

FIG. 2. A corner plot of the Bayesian analysis performed on the ROI showing the (a) two-peak (doublet) and (b) three-peak (triplet) model. The off-diagonals show the correlations between the parameters.

where a temperature parameter, β, was included to modify the likelihood calculation to L^β for each MCMC sample as outlined in Ref. [28] and discussed in Ref. [29]. Therefore with $\beta = 0$ the prior is sampled, and with $\beta = 1$ the posterior likelihood landscape is explored. An exponential ladder of β parameters was used to calculate the running average of an energy-like value,

$$\langle E_L(\beta)\rangle = -\ln\langle L\rangle_\beta.$$

The functions for the doublet and triplet model are plotted in Fig. 3. The resulting integration of $E_L(\beta)$ provides the Bayes Factor with

$$\ln(B_{\text{model}}) = -\int_0^1 \langle E_L(\beta)\rangle d\beta.$$

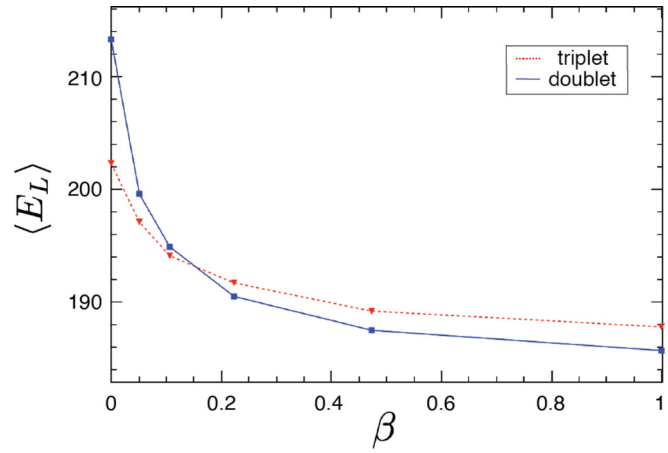

FIG. 3. The Bayes factor for each model was calculated by thermodynamic annealing. The resulting $\langle E_L\rangle$ for the different temperature parameters used is presented.

When comparing the calculated Bayes factors between the proposed doublet and triplet models we find a 1 : 1 ratio. To disentangle which is the preferred model we also calculated the Bayesian complexity, C_b, as defined in Ref. [30]. We find C_b(doublet) = 3.3 and C_b(triplet) = 3.0, which suggests that our data cannot fully discriminate between the two models. In fact, we interpret this to mean that our data in the ROI can only effectively determine three parameters of our model. Therefore it is very likely that there are other transitions present within the ROI.

A. Proton separation energy of ^{73}Rb

However, we apply Occam's razor and report values obtained with the simpler doublet model which provides a well-constrained energy for the lowest-energy peak in the β-delayed proton spectrum of ^{73}Sr. From this analysis the resulting proton separation energy of ^{73}Rb using the doublet model, after applying a β-summing correction (110 ± 15 keV) found from GEANT4 simulations of the detector setup [31] as well as LISE++ simulations of the implant depth distribution and accounting for the defect in measuring the recoil nucleus' energy [23], is determined to be $S(p) = -640(40)$ keV. Since the posterior probability for the low energy peak approximately reduced to a Gaussian, the error reported is 1σ of an approximate Gaussian added in quadrature with the β-summing uncertainty. Using the value of $Q_p = 3.85(3)$ MeV for ^{73}Rb*(IAS) and the new value of S_p, we find an excitation energy of $E_x = 3.21(5)$ MeV for ^{73}Rb*(IAS).

Furthermore, in the β decay of ^{73}Sr some population of the ^{73}Rb ground state is expected given the large Q_{β^+} and that the ground-state spin of ^{73}Rb from mirror symmetry, $J^\pi = 3/2^-$, should allow Gamow-Teller transitions. It is possible that a low-lying excited state is predominately populated instead, given the observation that ^{73}Sr has a $J^\pi = 5/2^-$ ground state. It is well established that there are nearly degenerate nuclear shapes in this region of the chart, or shape coexistence, particularly in ^{73}Br and ^{72}Kr [32–35]. Therefore it could also be the case that ^{73}Rb has a different ground state than its mirror

^{73}Kr, which would complicate an interpretation of the masses. Given these circumstances and the results of our Bayesian analysis, our presented separation energy can be considered a lower limit on the proton separation energy. This stringent lower limit on the separation energy is consistent with previous calculations assuming mirror symmetry holds for ^{73}Rb, informed by upper limits on the lifetime [22]. Since the error of our reported value encompasses the previous limits within 5σ, our result provides a firm determination for the proton separation energy of ^{73}Rb.

IV. IMME FOR $A = 73$ ISOBAR

Our result allows for a direct comparison of the $T = 1/2$ doublet of ^{73}Rb and ^{73}Kr for studies of isospin symmetry using the ground states of mirror pairs [36]. Deeply related, are studies of the isobaric multiplet mass equation (IMME) [37–39], which has proved to be a useful predictor of masses for nuclei near the $N = Z$ line of the chart of nuclides. For the $T = 1/2$ doublet of ^{73}Rb and ^{73}Kr we find that the b coefficient of the IMME, defined by the differences in mass excesses [37,38], to be $b = -10.542(40)$ MeV. This is surprisingly close to systematic predictions from studies of the IMME across the chart. In particular, Ref. [38] predicts a value of $b = -10.596(16)$ MeV from their global fit, which is encompassed by our measurement error.

Furthermore, with the excitation energy of the $J^\pi = 5/2^-$ IAS state in ^{73}Rb well determined, another piece of information has been added for studies of the IMME in $T = 3/2$ quartets. Such a study is complicated by the observation that the ground-state spins of ^{73}Sr and ^{73}Br differ, as a proper determination of the IMME would require data on the sets of both $J^\pi = 5/2-$ and $J^\pi = 1/2^-$ states throughout the $A = 73$ quartet. There is also an issue that the IASs in ^{73}Rb and ^{73}Kr may be slightly isospin-mixed states. Certainly this must be the case in ^{73}Rb, considering that it predominately decays by isospin-forbidden proton emission [40]. Isospin mixing typically manifests as an increase in the overall width of the resonance, but can result in a fragmentation of the IAS [41]. In any case, these effects occur on a level of precision that our measurement cannot assess.

However, we can provide a better constraint on the mass of ^{73}Sr using reasonable assumptions on the mirror energy differences between the IASs in ^{73}Rb and ^{73}Kr. The work on the systematics of the IMME previously mentioned [38], provides a compilation of b coefficients for many systems. From this we can deduce an estimate of the shift in b, or Δb, between the $T = 1/2$ and $T = 3/2$ systems along the $A = 73$ isobar based on previous data. For this study we took the differences in b between $T = 1/2$ ground states and the corresponding $T = 3/2$ systems for $19 \leqslant A \leqslant 37$. The low mass systems were not included, since the energy differences between levels are more sensitive to shell effects. This is also why we excluded the $A = 17$ and $A = 40$ systems from this study, since these are near shell closures. From these differences we find a sample mean of $\langle \Delta b \rangle = 6.2$ keV with a sample standard deviation of $\sigma_{\Delta b} = 107$ keV. Although this overlooks some systematic effects (e.g., the level densities are higher in heavier nuclei and we expect the IASs to be much lower in excitation energy) and the sample size is relatively small, we believe this study gives a conservative estimate for the IMME. Using these values, our estimate for the excitation energy for the $T = 3/2$ IAS in ^{73}Kr is $E_x = 3.204(118)$ MeV, where the error uses the sample standard deviation added in quadrature with our measurement error. When incorporating this value into a fit of the IMME (starting from the 27-keV $J^\pi = 5/2-$ state in ^{73}Br), one finds the mass excess of ^{73}Sr to be $\Delta M(^{73}\mathrm{Sr}) = -31.98(36)$, which is close to value from the 2016 Atomic Mass Evaluations (AME) of $\Delta M(^{73}\mathrm{Sr}) = -31.95(40)$ MeV [42]. This is not at all surprising considering that we have not considered any state dependent effects on the energy shifts of the IASs in ^{73}Rb and ^{73}Kr, but we have improved the overall estimate. Figure 4 shows the results of the IMME fit, and compares the extrapolated limits to the AME value.

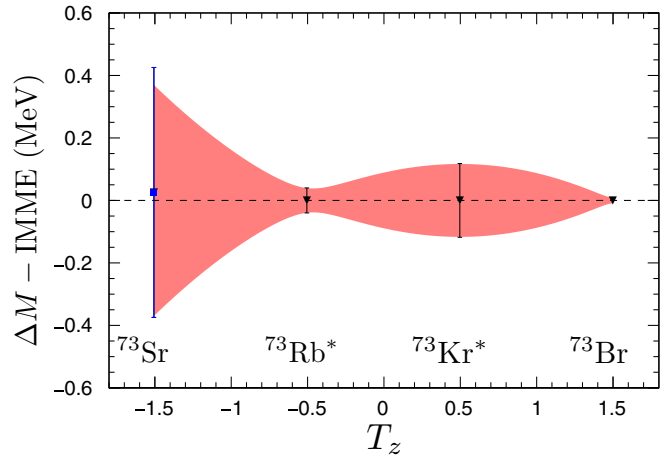

FIG. 4. The 1-σ confidence interval (red shaded area) from the IMME fit using the measured proton separation energy of ^{73}Rb as well as the empirically deduced distribution of mirror energy differences. The black triangles and error bars, show the limits used in the IMME fit, while the blue square shows the current limits for the mass excess of ^{73}Sr from the AME.

A. log(ft) of ^{73}Sr β decay

From these findings we can update the log(ft) previously provided for the β decay of ^{73}Sr. The previous value relied on the lowest-energy peak in the previous spectrum being identified as the proton separation energy. With the updated proton separation energy providing an excitation energy for ^{73}Rb*(IAS) of $E_x = 3.21(5)$ MeV, the better constrained mass excess of ^{73}Sr derived from the IMME, and our previous determination of the lifetime, $t_{1/2}(^{73}\mathrm{Sr}) = 23.1(1.4)$ ms, gives a log(ft) = 3.32(10), which is still consistent with the conservation of isobaric-spin. This value replaces the earlier estimate of 3.45(6) from our previous paper [23]. The measured population for the lowest energy peak of 2(1)% gives a log(ft) = 5.4(2) which is consistent with allowed Gamow-Teller transitions in this region of the chart [43], supporting that this peak corresponds to the population of a $J^\pi = 3/2^-$ ground state of ^{73}Rb. If the two counts above background below 600 keV in Fig. 1 correspond to ground state population, this would give

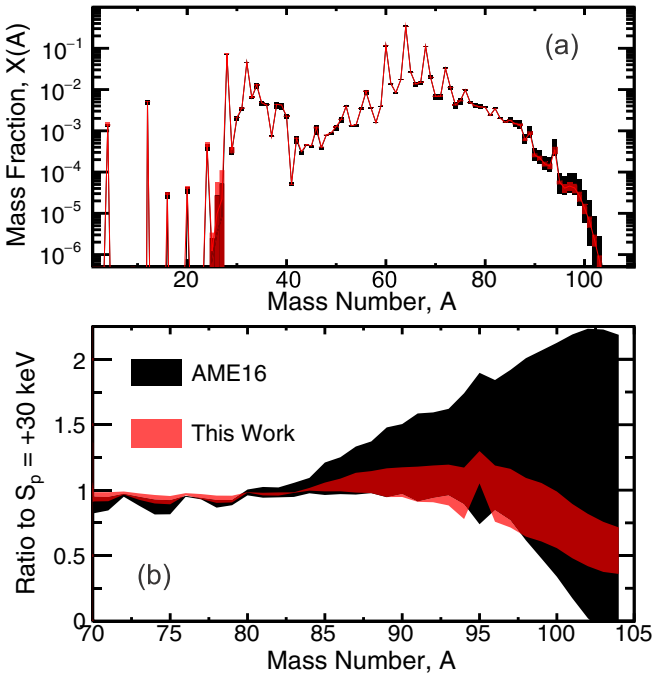

FIG. 5. (a) Ashes from XRB model calculations for $S(p)$ of ^{73}Rb $\pm 3\sigma$ for the 2016 AME (black) and our result $\pm 3\sigma$ (red). (b) Ratio of the results from (a) to the $X(A)$ of calculations with $S(p) = 30$ keV for high-A ashes. Our result overlaps the lower $|S_p|$ portion of the AME predictions. Uncertainty bands include fluctuations due to burst-to-burst scatter near the end of the burst sequence.

a branching of 0.6(4)%. This branching ratio corresponds to a $\log(ft) \geqslant 5.9$ suggesting that such a transition is forbidden. If this were the case then the ground state of ^{73}Rb must differ from its mirror ^{73}Kr, which does not seem likely since it does not have a nearly degenerate ground state like ^{73}Br. From this investigation of the possible decay matrix elements, along with previous upper limits to the proton separation energy, we conclude that the lowest energy proton group is the transition ^{73}Rb(g.s.) $\rightarrow$ ^{72}Kr(g.s.).

V. INFLUENCE OF ^{73}Rb $S(p)$ ON X-RAY BURSTS

With the better determined separation energy of ^{73}Rb, we also performed state-of-the-art x-ray burst model calculations to assess the impact of our result on the composition of ashes in accreting neutron stars following Type I x-ray bursts. One-dimensional x-ray burst model calculations, following the nuclear burning and hydrodynamic evolution induced by accretion on a neutron star envelope, were performed with the code MESA [44]. Calculations were performed as described in Ref. [45], using that work's best-fit conditions for the year 2007 x-ray bursting epoch of the accreting neutron star source GS 1826-24 [46], where the ashes were evaluated as described in Ref. [47]. To ensure convergence of the ashes and overcome compositional inertia [7], the envelope composition was evaluated after a sequence of 21 bursts.

Figure 5(a) shows the mass-fraction $X(A)$ distribution of the neutron star envelope for a range of $S(p)$, while Fig. 5(b) shows the ratio of the mass-fraction for a choice of $S(p)$ relative to the most-bound proton separation energy of ^{73}Rb considered. The black band in the figure corresponds to the 2016 AME [42] proton separation energy extrapolation for ^{73}Rb with an uncertainty of ± 3 standard deviations, where $S(p) = -570 \pm 600$ keV for 3σ, yielding the most-bound separation energy of ^{73}Rb $+30$ keV. The red band corresponds to the new result with an uncertainty of $\pm 3\sigma$ [$S(p) = -640 \pm 120$ keV]. Both bands include an uncertainty contribution due to fluctuations in $X(A)$ from burst-to-burst for the last four bursts in the sequence.

Figure 5(b) focuses on the abundance region around $A = 70$ and above. In particular, $X(A)$ for $A \geqslant 102$ are especially interesting, since these play a critical role in setting the thermal conductivity of the accreted neutron star crust [17]. As x-ray burst ashes are buried in the neutron star crust, reactions in the crust funnel nuclides into equilibrium isotopes with magic neutron numbers. Lau *et al.* [17] found that, when using the FRDM2012 [48] mass model, isotopes are ultimately transmuted into either ^{40}Mg, ^{70}Ca, or ^{116}Se, depending on the initial A of the isotope in the x-ray burst ashes, where similar funneling occurs to different equilibrium isotopes for different nuclear mass models [49]. When the ashes contain material with $A \geqslant 102$, the $N = 82$ equilibrium isotope is present in the crust. This enhances the variance of nuclear charge for isotopes present in the crust, which corresponds to an enhancement of the crust impurity: $Q_{\rm imp} \equiv n_{\rm ion}^{-1} \sum_j n_j (Z_j - \langle Z \rangle)^2$, where Z_j is the nuclear charge of species j, with average $\langle Z \rangle$, and the number density of ions $n_{\rm ion}$ and species n_j, respectively [50].

Modifications to the accreted neutron star crust impurity are significant due to the impact on the inner crust thermal conductivity $K \propto Q_{\rm imp}$ [51]. A neutron star for which accretion ceases after an outburst of months or years, known as a cooling transient, cools as the crust returns to thermal equilibrium. The more impure crust has a reduced thermal conductivity, leading to increased neutron star crust cooling times [52]. However, crust cooling times are also linked to other neutron star properties, such as the neutron star compactness via the time-dilation from surface gravitational redshift. Therefore, accurate predictions of the crust impurity are necessary to constrain model-observation comparisons for cooling transient neutron stars, comparisons which provide unique insight into neutron star structure [6,53].

One can see that the mass-fraction uncertainty in this region is drastically reduced given our result, demonstrating the importance of measuring nuclear properties for nuclear reaction network calculations. The uncertainty in $X(102)$, which dominates the sum of $X(A)$ for $A \geqslant 102$, reduced from about a factor of 100 to roughly a factor of 2. The new measurement for the separation energy of ^{73}Rb eliminates the proton-separation energy as an uncertainty for the crust impurity, as the current uncertainty is dominated by burst-to-burst fluctuations. We note that for the set of astrophysical conditions modeled here, the ultimate impact on $Q_{\rm imp}$ will be minor, as the sum of $X(A)$ for $A \geqslant 102$ is small. However, the impact is expected to be significant for more extreme conditions leading to heavier burst ashes, e.g. the extreme case of Ref. [54]. Our work also highlights the somewhat counterintuitive result that a more negative $S(p)$ for ^{73}Rb,

i.e. a stronger waiting-point, leads to enhanced abundances of nuclides further along in the *rp*-process path. A small $|S(p)|$ enables an equilibrium abundance of ^{73}Rb to be established, and thus for each decay of this nucleus, proton-capture will replenish the equilibrium abundance, essentially tying-up protons in the replenishment rather than synthesizing higher-A nuclides [2].

VI. CONCLUSION

In summary, from recent data on the β-delayed proton spectrum of ^{73}Sr we have found a proton separation energy for ^{73}Rb of $S(p) = -640(40)$ keV, slightly more unbound than systematic predictions. Recent experiments have also confirmed the unbound nature of ^{73}Rb [22], cementing ^{72}Kr as a waiting-point nucleus. Our result coupled with these previous limits provides a precise determination on proton separation energy sufficient for the study of astrophysical scenarios. We find that the mass fraction of $A > 102$ is significantly enhanced with ^{73}Rb being further unbound. Indeed it is remarkable that a 0.5–1 MeV discrepancy for the mass of ^{73}Rb can have such a significant impact on the products of the *rp* process. Given the proximity of the latter half of the *rp*-process path to the proton dripline and the reliance of x-ray burst model calculations on mass estimates from the AME [54,55], our results suggest mass measurements of $A \geqslant 73$ nuclei along the proton dripline will be required to provide accurate impurity distributions within accreting neutron stars, and therefore also accurate cooling models for their crusts.

ACKNOWLEDGMENTS

We would like to specifically thank Tom Ginter for his effort in providing the ^{73}Sr beam used in the experiment and Witold Nazarewicz for his invaluable discussions. We acknowledge support from the US DOE, Office of Science, Office of Nuclear Physics under Awards No. DE-FG02-94ER40848 (UML), No. DE-AC02-06CH11357 (ANL), No. DE-SC0013365 (NSCL), as well as No. DE-FG02-88ER40387 and No. DE-SC0019042 (OU); the NNSA through Awards No. DENA0003180 (NSSC), No. DE-NA0000979 (NSSC), No. DE-NA0003221, and/or No. DE-NA0002132; and the NSF under Contract No. PHY-1-102511.

[1] R. K. Wallace and S. E. Woosley, Astrophys. J. Suppl. Ser. **45**, 389 (1981).
[2] L. van Wormer, J. Görres, C. Iliadis, M. Wiescher, and F. K. Thielemann, Astrophys. J. **432**, 326 (1994).
[3] H. Schatz, A. Aprahamian, J. Görres, M. Wiescher, T. Rauscher, J. Rembges, F.-K. Thielemann, B. Pfeiffer, P. Möller, K.-L. Kratz, H. Herndl, B. Brown, and H. Rebel, Phys. Rep. **294**, 167 (1998).
[4] J. L. Fisker, V. Barnard, J. Görres, K. Langanke, G. Martínez-Pinedo, and M. C. Wiescher, At. Data Nucl. Data Tables **79**, 241 (2001).
[5] B. A. Brown, R. R. C. Clement, H. Schatz, A. Volya, and W. A. Richter, Phys. Rev. C **65**, 045802 (2002).
[6] Z. Meisel, A. Deibel, L. Keek, P. Shternin, and J. Elfritz, J. Phys. G **45**, 093001 (2018).
[7] S. E. Woosley, A. Heger, A. Cumming, R. D. Hoffman, J. Pruet, T. Rauscher, J. L. Fisker, H. Schatz, B. Brown, and M. Wiescher, Astrophys. J. Suppl. Ser. **151**, 75 (2004).
[8] D. Rodríguez, V. S. Kolhinen, G. Audi, J. Äystö, D. Beck, K. Blaum, G. Bollen, F. Herfurth, A. Jokinen, A. Kellerbauer, H. J. Kluge, M. Oinonen, H. Schatz, E. Sauvan, and S. Schwarz, Phys. Rev. Lett. **93**, 161104 (2004).
[9] J. A. Clark, G. Savard, K. S. Sharma, J. Vaz, J. C. Wang, Z. Zhou, A. Heinz, B. Blank, F. Buchinger, J. E. Crawford, S. Gulick, J. K. P. Lee, A. F. Levand, D. Seweryniak, G. D. Sprouse, and W. Trimble, Phys. Rev. Lett. **92**, 192501 (2004).
[10] J. A. Clark, K. S. Sharma, G. Savard, A. F. Levand, J. C. Wang, Z. Zhou, B. Blank, F. Buchinger, J. E. Crawford, S. Gulick, J. K. P. Lee, D. Seweryniak, and W. Trimble, Phys. Rev. C **75**, 032801(R) (2007).
[11] A. Kankainen, V.-V. Elomaa, T. Eronen, D. Gorelov, J. Hakala, A. Jokinen, T. Kessler, V. S. Kolhinen, I. D. Moore, S. Rahaman, M. Reponen, J. Rissanen, A. Saastamoinen, C. Weber, and J. Äystö, Phys. Rev. C **82**, 034311 (2010).
[12] A. M. Rogers, M. A. Famiano, W. G. Lynch, M. S. Wallace, F. Amorini, D. Bazin, R. J. Charity, F. Delaunay, R. T. de Souza, J. Elson, A. Gade, D. Galaviz, M.-J. van Goethem, S. Hudan, J. Lee, S. Lobastov, S. Lukyanov, M. Matoš, M. Mocko, H. Schatz, D. Shapira, L. G. Sobotka, M. B. Tsang, and G. Verde, Phys. Rev. Lett. **106**, 252503 (2011).
[13] X. L. Tu, H. S. Xu, M. Wang, Y. H. Zhang, Y. A. Litvinov, Y. Sun, H. Schatz, X. H. Zhou, Y. J. Yuan, J. W. Xia, G. Audi, K. Blaum, C. M. Du, P. Geng, Z. G. Hu, W. X. Huang, S. L. Jin, L. X. Liu, Y. Liu, X. Ma, R. S. Mao, B. Mei, P. Shuai, Z. Y. Sun, H. Suzuki, S. W. Tang, J. S. Wang, S. T. Wang, G. Q. Xiao, X. Xu, T. Yamaguchi, Y. Yamaguchi, X. L. Yan, J. C. Yang, R. P. Ye, Y. D. Zang, H. W. Zhao, T. C. Zhao, X. Y. Zhang, and W. L. Zhan, Phys. Rev. Lett. **106**, 112501 (2011).
[14] M. D. Santo, Z. Meisel, D. Bazin, A. Becerril, B. Brown, H. Crawford, R. Cyburt, S. George, G. Grinyer, G. Lorusso, P. Mantica, F. Montes, J. Pereira, H. Schatz, K. Smith, and M. Wiescher, Phys. Lett. B **738**, 453 (2014).
[15] S. Gupta, E. F. Brown, H. Schatz, P. Möller, and K.-L. Kratz, Astrophys. J. **662**, 1188 (2007).
[16] A. A. Valverde, M. Brodeur, G. Bollen, M. Eibach, K. Gulyuz, A. Hamaker, C. Izzo, W. J. Ong, D. Puentes, M. Redshaw, R. Ringle, R. Sandler, S. Schwarz, C. S. Sumithrarachchi, J. Surbrook, A. C. C. Villari, and I. T. Yandow, Phys. Rev. Lett. **120**, 032701 (2018).
[17] R. Lau, M. Beard, S. S. Gupta, H. Schatz, A. Afanasjev, E. F. Brown, A. Deibel, L. R. Gasques, G. W. Hitt, W. R. Hix *et al.*, Astrophys. J. **859**, 62 (2018).
[18] N. N. Weinberg, L. Bildsten, and H. Schatz, Astrophys. J. **639**, 1018 (2006).
[19] A. Parikh, J. José, F. Moreno, and C. Iliadis, Astrophys. J. Suppl. Ser. **178**, 110 (2008).
[20] A. Jokinen, M. Oinonen, J. Äystö, P. Baumann, F. Didierjean, P. Hoff, A. Huck, A. Knipper, G. Marguier, Y. N. Novikov, A. V. Popov, M. Ramdhane, D. M. Seliverstov, P. Van Duppen,

G. Walter, and the ISOLDE Collaboration, Z. Phys. A **355**, 227 (1996).
[21] R. Pfaff, D. J. Morrissey, W. Benenson, M. Fauerbach, M. Hellström, C. F. Powell, B. M. Sherrill, M. Steiner, and J. A. Winger, Phys. Rev. C **53**, 1753 (1996).
[22] H. Suzuki, L. Sinclair, P.-A. Söderström, G. Lorusso, P. Davies, L. S. Ferreira, E. Maglione, R. Wadsworth, J. Wu, Z. Y. Xu, S. Nishimura, P. Doornenbal, D. S. Ahn, F. Browne, N. Fukuda, N. Inabe, T. Kubo, D. Lubos, Z. Patel, S. Rice, Y. Shimizu, H. Takeda, H. Baba, A. Estrade, Y. Fang, J. Henderson, T. Isobe, D. Jenkins, S. Kubono, Z. Li, I. Nishizuka, H. Sakurai, P. Schury, T. Sumikama, H. Watanabe, and V. Werner, Phys. Rev. Lett. **119**, 192503 (2017).
[23] D. E. M. Hoff, A. M. Rogers, S. M. Wang *et al.*, Nature **580**, 52 (2020).
[24] D. Morrissey, B. Sherrill, M. Steiner, A. Stolz, and I. Wiedenhoever, Nucl. Instrum. Methods Phys. Res. B **204**, 90 (2003); 14th International Conference on Electromagnetic Isotope Separators and Techniques Related to their Applications.
[25] D. Bazin, V. Andreev, A. Becerril, M. Doléans, P. Mantica, J. Ottarson, H. Schatz, J. Stoker, and J. Vincent, Nucl. Instrum. Methods Phys. Res. A **606**, 314 (2009).
[26] See Supplemental Material at http://link.aps.org/supplemental/10.1103/PhysRevC.102.045810 for a discussion of the event-by-event trace analysis reducing the background of the ^{73}Sr data.
[27] D. Foreman-Mackey, D. W. Hogg, D. Lang, and J. Goodman, Publ. Astron. Soc. Pac. **125**, 306 (2013).
[28] P. M. Goggans and Y. Chi, AIP Conf. Proc. **707**, 59 (2004).
[29] M. A. Clyde, J. O. Berger, F. Bullard, E. B. Ford, W. H. Jefferys, R. Luo, R. Paulo, and T. Loredo, in *Statistical Challenges in Modern Astronomy IV*, Astronomical Society of the Pacific Conference Series, edited by G. J. Babu and E. D. Feigelson (ASP, 2007), Vol. 371, p. 224.
[30] R. Trotta, Contemp. Phys. **49**, 71 (2008).
[31] Z. Meisel, M. del Santo, H. Crawford, R. Cyburt, G. Grinyer, C. Langer, F. Montes, H. Schatz, and K. Smith, Nucl. Instrum. Methods Phys. Res. A **844**, 45 (2017).
[32] B. Wörmann, J. Heese, K. Lieb, L. Lühmann, F. Raether, D. Alber, H. Grawe, and B. Spellmeyer, Z. Phys. A: At. Nucl. **322**, 171 (1985).
[33] J. Heese, N. Martin, C. J. Gross, W. Fieber, K. P. Lieb, A. Kuhnert, K. H. Maier, and X. Sun, Phys. Rev. C **41**, 1553 (1990).
[34] A. Gade, D. Bazin, A. Becerril, C. M. Campbell, J. M. Cook, D. J. Dean, D.-C. Dinca, T. Glasmacher, G. W. Hitt, M. E. Howard, W. F. Mueller, H. Olliver, J. R. Terry, and K. Yoneda, Phys. Rev. Lett. **95**, 022502 (2005).
[35] K. Wimmer, T. Arici, W. Korten, P. Doornenbal, J.-P. Delaroche, M. Girod, J. Libert, T. Rodríguez, P. Aguilera, A. Algora *et al.*, Eur. Phys. J. A **56**, 159 (2020).
[36] P. Bączyk, W. Satuła, J. Dobaczewski, and M. Konieczka, J. Phys. G: Nucl. Part. Phys. **46**, 03LT01 (2019).
[37] W. Benenson and E. Kashy, Rev. Mod. Phys. **51**, 527 (1979).
[38] Y. H. Lam, B. Blank, N. A. Smirnova, J. B. Bueb, and M. S. Antony, At. Data Nucl. Data Tables **99**, 680 (2013).
[39] M. MacCormick and G. Audi, Nucl. Phys. A **925**, 61 (2014).
[40] N. A. Smirnova, B. Blank, B. A. Brown, W. A. Richter, N. Benouaret, and Y. H. Lam, Phys. Rev. C **95**, 054301 (2017).
[41] V. Tripathi, S. L. Tabor, A. Volya, S. N. Liddick, P. C. Bender, N. Larson, C. Prokop, S. Suchyta, P.-L. Tai, and J. M. VonMoss, Phys. Rev. Lett. **111**, 262501 (2013).
[42] M. Wang, G. Audi, F. G. Kondev, W. Huang, S. Naimi, and X. Xu, Chin. Phys. C **41**, 030003 (2017).
[43] S. Raman and N. B. Gove, Phys. Rev. C **7**, 1995 (1973).
[44] B. Paxton, P. Marchant, J. Schwab, E. B. Bauer, L. Bildsten, M. Cantiello, L. Dessart, R. Farmer, H. Hu, N. Langer, R. H. D. Townsend, D. M. Townsley, and F. X. Timmes, Astrophys. J. Suppl. Ser. **220**, 15 (2015).
[45] Z. Meisel, Astrophys. J. **860**, 147 (2018).
[46] D. K. Galloway, A. J. Goodwin, and L. Keek, Pub. Astron. Soc. Aust. **34**, E019 (2017).
[47] Z. Meisel, G. Merz, and S. Medvid, Astrophys. J. **872**, 84 (2019).
[48] P. Möller, W. D. Myers, H. Sagawa, and S. Yoshida, Phys. Rev. Lett. **108**, 052501 (2012).
[49] N. N. Shchechilin and A. I. Chugunov, MNRAS **490**, 3454 (2019).
[50] N. Itoh and Y. Kohyama, Astrophys. J. **404**, 268 (1993).
[51] E. F. Brown and A. Cumming, Astrophys. J. **698**, 1020 (2009).
[52] D. Page and S. Reddy, Phys. Rev. Lett. **111**, 241102 (2013).
[53] R. Wijnands, N. Degenaar, and D. Page, J. Astrophys. Astron. **38**, 49 (2017).
[54] H. Schatz and W. J. Ong, Astrophys. J. **844**, 139 (2017).
[55] H. Schatz, A. Aprahamian, V. Barnard, L. Bildsten, A. Cumming, M. Ouellette, T. Rauscher, F.-K. Thielemann, and M. Wiescher, Phys. Rev. Lett. **86**, 3471 (2001).